J|A|C|S
COMMUNICATIONS

Published on Web 02/24/2006

Interfacial Thermocapillary Vortical Flow for Microfluidic Mixing

Ramanathan Muruganathan, Yi Zhang, and Thomas M. Fischer*

Department of Chemistry and Biochemistry, Florida State University, Tallahassee, Florida

Received October 7, 2005; E-mail: tfischer@chem.fsu.edu

Vortical flow, a flow with finite vorticity, is important both in laminar[1] and in turbulent[2] mixing of two highly viscous fluids.[3] An outstanding issue in a variety of microfluidic operations[4,5] is the efficient mixing of liquid-phase chemical species. Due to the small length scales, turbulent mixing, which is extensively utilized in larger scale flows, cannot be achieved, and new schemes must be developed. Miniaturization of fluid devices increases the importance of interfacial quasi-two-dimensional flow as compared to large scale bulk flow. The reduced dimensionality of the flow on one hand suppresses the mixing by eliminating the possibilities of vortex stretching;[6] on the other hand, it opens new routes for mixing via interfacial stresses that drive the flow. Mixing often is achieved via stirring, and one may characterize the stirring by the magnitude of the vorticity that is the local angular velocity of rotation of the fluid. Vortical flow at low Reynolds numbers[7,8] is an important characteristic for the efficient mixing on microfluidic lab-on-a-chip devices[4,5] outside the turbulent regime.

Here we report on the formation of vortical flow in a low Reynolds number, quasi-two-dimensional Langmuir monolayer at the air/water interface that might serve as a microfluidic mixer. For the experiment, we need a quasi-two-dimensional pump to create the flow, and we need solid objects to obstruct the flow. As a microfluidic pump we use an IR laser that is focused on the air/water surface.[9] The laser locally heats the monolayer as well as the water underneath to create a thermal gradient. Surface tension gradients produced by the temperature-dependent surface tension $\gamma(T)$ open a cavitation gas bubble in the liquid-expanded (LE) phase of the Langmuir monolayer[10,11] (Figure 1). The cavitation occurs when the drop in surface tension due to the heating exceeds the surface pressure of the LE-phase monolayer. The line tension $\lambda(T)$ between the gaseous phase of the 2D bubble and its LE surroundings also varies with temperature. If spontaneous symmetry breaking displaces the bubble from the laser focus, then the LE/gas boundary closer to the focus will be hotter and the cavitation bubble boundary exerts a thermocapillary stress that sets the liquid into motion[12,13] and amplifies the displacement and the flow. We use the thermocapillary flow of the bubble to pump the LE-phase past giant folds[14−18] (Figure 1, top left) that obstruct the flow like a solid object. The folds are produced by compressing a 1:1 mixture of a L-α-dipalmitoylphosphatidylcholine (DPPC) and a 1,2-dipalmitoyl-*sn*-glycero-3- {phosphor-L-serine} (DPPS) monolayer beyond its collapse pressure. Surfactant material irreversibly aggregates into folds in the water below the monolayer, and a reexpansion of the monolayer leads to a coexistence of the LE and gas phase with the folds that cut the LE into disjoined sections.[19] Thermocapillary flow of sufficient strength breaks these folds into two pieces. We then observe the flow of the monolayer beyond one of the broken ends of the fold (Figure 1, bottom right). When the flow passes the fold, we observe a separation of the boundary layer from the folds. The streamlines are visualized by the tail of the cavitation gas bubble that follows the flow and creates a contrast to the LE phase in the fluorescence microscope images (Figure 1, bottom left and right and videos in the Supporting Information). Instead of clinging to the folds, the streamlines extend past the fold and bend toward the fold only after a distance of 100 μm.

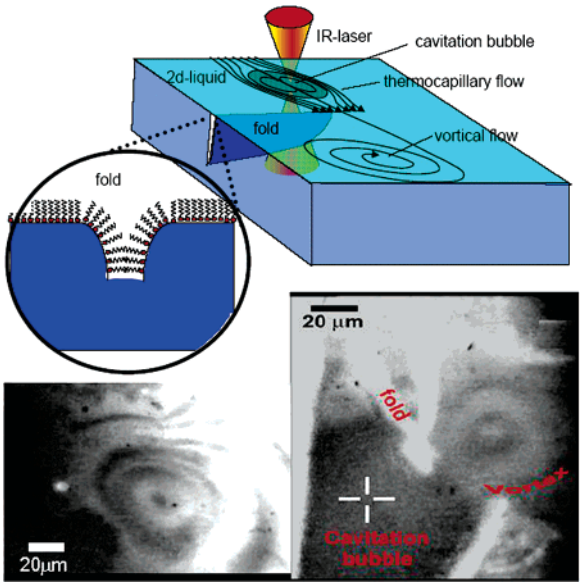

Figure 1. Top right: Schematics of the experiment producing the vortical flow. Top left: Detailed schematics of the giant fold. Bottom right: Fluorescence microscope image of a mixed DPPC−DPPS monolayer with folds (bright), cavitation bubble (dark) created in the laser focus (cross hair), and vortical flow behind a fold. Bottom left: Close-up view of a fluorescence microscope image of a different vortex.

The result is a vortex of radius $\approx$ 100 μm with streamlines circling around the center with velocity **u**. Using polar coordinates r,ϑ centered at the vortex, we measure the azimuthal velocity component u_ϑ of the monolayer around the vortex by following frame-by-frame characteristic small gas bubbles that are advected by the flow. The vorticity $\boldsymbol{\omega} = \nabla \times \mathbf{u}$ of such a vortex calculated from u_ϑ is depicted as a function of the radius r measured from the center of the vortex (Figure 2). The vorticity shows a bipolar behavior with a positive vorticity for $r < R = 50$ μm and a negative vorticity farther outside. The order of magnitude of the vorticity is in the range $\omega \approx 1\ s^{-1}$. Using the density $\rho = 1$ g cm^{-3} and viscosity $\eta = 10^{-3}$ Nsm^{-2} of water, we find that the Reynolds number $Re = \rho\omega R^2/\eta \ll 1$ is very small. The hydrodynamics is therefore governed by the equations of creeping flow. Since the viscous stresses associated with the flow are too small to cause any surface compression $\kappa_s \eta u \ll 1$ (κ_s is the surface compressibility), the monolayer on top of the air/water interface can be treated as incompressible.[20] There is no advection of vorticity under these circumstances, and the source of the vorticity must be an effective torque exerted on the surface. The surface torque is a linear

10.1021/ja0566883 CCC: $33.50

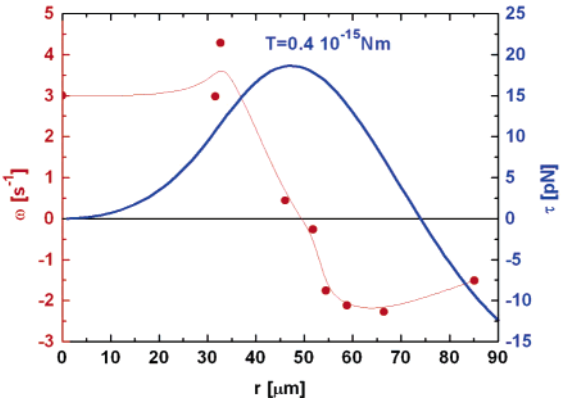

Figure 2. Vorticity (red) of the vortex of Figure 1 (bottom left) as a function of the radial distance from the vortex center. The blue line is the torque density deconvoluted from the red data according to eq 1. The total torque of $T = 0.4 \times 10^{-15}$ Nm concentrates around $r = R = 50$ μm, where the vorticity changes sign.

functional of the vorticity profile at the surface, and we may deconvolute the torque from the vorticity data via:

$$\tau(r) = -4\eta r^2 \frac{\mathrm{d}}{\mathrm{d}r}\int_0^\infty \mathrm{d}r'\omega(r')\frac{r'}{r+r'}K\left(\frac{2\sqrt{rr'}}{r+r'}\right) \qquad (1)$$

where $\tau(r)$ is the surface torque density, $T = \int \mathrm{d}r\, \tau(r)$ is the total torque, and K is the complete elliptic integral of the first kind.[21] The torque profile as a function of the radial distance from the vortex center obtained from the vorticity data via eq 1 is displayed in Figure 2. We find a total torque of the order $T = 0.4 \times 10^{-15}$ Nm, most of which is located at the distance $R \approx 50$ μm, where the vorticity changes sign. A change of vorticity at the location of the source of the vortex is expected since the velocity gradient will point in opposite directions on each side of the torque source. The magnitude of the torque density ($\tau \approx 10$ pN) is of comparable magnitude as the forces required for manipulating the monolayer with optical tweezers.[9] The torque density arises from physical origins that exclude viscous traction from the subphase and surface pressure gradients. The physical reason for the torque might be thermocapillary effects occurring in the region where the hot fluid from the bubble meets the cold fluid behind the fold. The vorticity created in this way stretches the LE and gaseous phase in the azimuthal direction and at the same time thins both phases in the radial direction. The precise nature of the fold should not matter, and the use of more stable obstacles such as a solid knife edge instead of the fold for a controlled mixing seems feasable. For the mixing to be useful, it is important that the vortical flow propagates to a certain depth into the bulk phase. We have not measured the penetration depth; however, the creeping flow equations suggest that the penetration depth is of the order of the lateral extension of the vortex.[21] The penetration depth therefore is expected to be in the typical order of magnitude (100 μm) of microfluidic channels. If the vortical flow could be maintained long enough to reach a radial thinning that would allow the interdiffusion of surfactants at the surface, then this technique would open a route for the effective two-dimensional microfluidic mixing at low Reynolds numbers.

In summary, we propose a simple way of achieving two-dimensional mixing via formation of the vortical flow behind the folds in a low Reynolds number Langmuir monolayer. The vortical flow in the quasi 2D system resembles eddies forming behind the objects in a high Reynolds number flow. The vortex is driven by a torque of the order $T = 10^{-15}$ Nm. The torque might originate from the thermocapillary stress between the hot fluid entering the area via the unblocked side of the fold and the cold water in the area shadowed by the fold.

Acknowledgment. Stimulating discussion with Walter Goldburg is highly acknowledged.

Supporting Information Available: Experimental setup, method, derivation of eq 1, a real time movie showing the interfacial thermocapillary vortical flow including the thermocapillary pump, the folds, and the vortex, and a real-time movie with a close-up view of a vortex (MPG, PDF). This material is available free of charge via the Internet at http://pubs.acs.org.

References

(1) Happel, J.; Brenner, H. *Low Reynolds number hydrodynamics*, 3rd ed.; Martinus Nijhoff Publishers: The Hague, 1983.
(2) Batchelor, G. K. *An introduction to fluid dynamics*; Cambridge University Press: New York, 2005.
(3) Ottino, J. M. *The kinematics of mixing: stretching, chaos, and transport*; Cambridge University Press: New York, 1989.
(4) Stone, H. A.; Strook, A. D.; Aidari, A. *Annu. Rev. Fluid Mech.* **2004**, *36*, 381.
(5) Squires, T. M.; Quake, S. R. *Rev. Mod. Phys.* **2005**, *77*, 977.
(6) Kellay, H.; Goldburg, W. I. *Rep. Prog. Phys.* **2002**, *65*, 845.
(7) Johnson, T. J.; Ross, D.; Locascio, L. E. *Anal. Chem.* **2002**, *74*, 45.
(8) Wiggins, S.; Ottino, J. M. *Philos. Trans. R. Soc. London, Ser. A* **2004**, *362*, 937.
(9) Wurlitzer, S.; Lautz, C.; Liley, M.; Duschl, C.; Fischer, T. M. *J. Phys. Chem. B* **2001**, *105*, 182.
(10) Khattari, Z.; Hatta, E.; Kurth, D. G.; Fischer, T. M. *J. Chem. Phys.* **2001**, *115*, 9923.
(11) Khattari, Z.; Steffen, P.; Fischer, T. M.; Bruinsma, R. *Phys. Rev. E* **2002**, *65*, 041603.
(12) Young, N. O.; Goldstein, J. S.; Block, M. J. *J. Fluid Mech.* **1959**, *6*, 350.
(13) Muruganathan, R. M.; Khattari, Z.; Fischer, T. M. *J. Phys. Chem. B* **2005**, *109*, 21772.
(14) Lipp, M.; Lee, K. Y. C.; Takamoto, D. Y.; Zasadzinski, J. A.; Waring, A. J. *Phys. Rev. Lett.* **1998**, *81*, 1650.
(15) Gopal, A.; Lee, K. Y. C. *J. Phys. Chem. B* **2001**, *105*, 10348.
(16) Lu, W. X.; Knobler, C. M.; Bruinsma, R. F.; Twardos, M.; Dennin, M. *Phys. Rev. Lett.* **2002**, *89*, 146107.
(17) Hatta, E.; Fischer, T. M. *J. Phys. Chem.* **2002**, *106*, 589.
(18) Ybert, C.; Lu, W. X.; Möller, G.; Knobler, C. M. *J. Phys. Chem. B* **2002**, *106*, 2004.
(19) Zhang, Y.; Fischer, T. M. *J. Phys. Chem. B* **2005**, *109*, 3442.
(20) Saffman, P. G.; Delbrück, M. *Proc. Natl. Acad. Sci. U.S.A.* **1975**, *72*, 3111.
(21) Details of the calculations and derivation of eq 1 are given in the Supporting Information, section S2.

JA0566883